SAND2007-8048C

Application of Raman/Rayleigh/LIF diagnostics in turbulent stratified flames

R. S. Barlow[a*], G. H. Wang[a], P. Anselmo-Filho[b], M.S. Sweeney[b], S. Hochgreb[b]

[a]*Sandia National Laboratories, Livermore, CA 94551-0969, USA*

[b]*Engineering Department, University of Cambridge, Cambridge CB2 1PZ, UK*

*Author for correspondence:
Robert Barlow
Sandia National Laboratories, MS-9051
PO Box 969, Livermore, CA 94551-0969, USA
email: barlow@sandia.gov
tel: 925-294-2688
fax: 925-294-2595

Submitted to the 32nd International Symposium on Combustion

Colloquium: Diagnostics

Short running title: Raman diagnostics in turbulent stratified flames

Estimated Length:

Text (format and measure)		3070
References (format and measure)		290
Table 1 (11 lines)		100
Table 2 (9 lines)		85
Fig. 1 (single column)	color in print	210
Fig. 2 (single column)	color in print	140
Fig. 3 (single column)		170
Fig. 4 (single column)		300
Fig. 5 (two column)		440
Fig. 6 (two column)		460
Fig. 7 (two column)	color in print	510
Total		5775

Affirmation: Cost of printing the designated color figures will be paid by the corresponding author, Robert Barlow, Sandia National Laboratories.

Application of Raman/Rayleigh/LIF diagnostics in turbulent stratified flames

R. S. Barlow[a*], G. H. Wang[a], P. Anselmo-Filho[b], M. Sweeney[b], S. Hochgreb[b]

[a]*Sandia National Laboratories, Livermore, CA 94551-0969, USA*

[b]*Engineering Department, University of Cambridge, Cambridge CB2 1PZ, UK*

Abstract

Stratified flames are common in practical combustion systems. However, relatively little is known about the detailed structure and dynamics of turbulent stratified flames. Multiscalar laser diagnostics, consisting of simultaneous line imaging of Raman scattering, Rayleigh scattering, and two-photon laser-induced fluorescence (LIF) of CO, combined with crossed planar imaging of OH LIF, are applied to turbulent premixed and stratified CH_4/air flames stabilized above a slot burner. A new detection system for the line-imaged measurements yields a resolution of 0.104 mm in the results for temperature, major species concentrations, and the local equivalence ratio. Results from premixed flames demonstrate that this diagnostic system is capable of resolving the internal structure of thin flames. In particular, the local equivalence ratio and the gradient in temperature are measured with good accuracy on a single-shot basis. Results from stratified flames reveal a broad range of instantaneous conditions, and show that significant gradients in equivalence ratio can occur within the instantaneous thermal thickness of turbulent stratified flames.

*Keywords***:** Stratified flames, Premixed flames, Turbulent combustion, Raman scattering

*Corresponding author: Tel.: +925-294-2688; fax: +925-294-2595

E-mail address: barlow@sandia.gov (R.S. Barlow)

1. Introduction

Many combustion systems for transportation and power generation operate in regimes where reactants are neither homogeneously mixed when a reaction front propagates through them (ideal premixed flame) nor segregated on two sides of a contiguous, nonpremixed reaction zone (ideal diffusion flame). Stratified combustion, in which a flame propagates through non-uniformly mixed reactants, is common in practical systems [1,2] and in model combustors that have been designed to study relevant phenomena at atmospheric pressure [3-5]. Computational models have been applied to such systems with some success [4-6]. However, fundamental questions regarding the structure and dynamics of turbulent stratified flames remain unanswered. DNS studies in two dimensions have provided useful insights [7,8], and recent experimental studies have begun to systematically investigate stratified flames [9-12].

A two-dimensional slot burner was developed at the University of Cambridge to allow for comparisons of turbulent premixed and stratified flames in a relatively simple geometry. Several flames with different levels of stratification and turbulence intensity have been studied using simultaneous planar imaging of acetone and OH [12]. Velocity measurements have also been made and will be reported separately. As a complement to these experiments, multiscalar measurements were obtained at Sandia for several premixed and stratified cases.

The objective of the present paper is to demonstrate the usefulness of simultaneous line-imaged Raman/Rayleigh/LIF measurements for probing the structure of turbulent stratified flames. The experimental facility used in the present work was developed to address the challenge of measuring mixture fraction dissipation and related quantities in turbulent nonpremixed and partially premixed hydrocarbon flames [13-15]. Stratified flames present diagnostic challenges similar to those of measuring scalar dissipation in nonpremixed flames,

requiring that the local state of mixing between fuel and oxidizer be measured with the best possible combination of precision and spatial resolution. Because Raman scattering is a relatively weak process, the spatial resolution achievable by most systems described in the literature is not sufficient to resolve the thin reaction zones in premixed or stratified flames. However, recent development of a new optical collection system for line-imaged Raman/Rayleigh/LIF measurements in the Turbulent Combustion Laboratory at Sandia has allowed significant improvement in the spatial resolution of multiscalar measurements. The present slot burner was the first research target of this new system and, to our knowledge, this is the first application of Raman-based multiscalar laser diagnostics to probe the internal scalar structure of turbulent stratified flames.

2. Experimental Methods

2.1. Slot burner and flame conditions

The slot burner shown in Fig. 1 was developed at the University of Cambridge [12] to allow fundamental investigation of turbulent stratified combustion in a simple experimental geometry that could also be addressed using direct numerical simulation (DNS). The burner consists of parallel slots supplied by two streams of independently controlled mixtures of methane and air, such that a turbulent mixing layer between these two streams develops above the center of the burner. Coflowing air is supplied through the outer slots. As illustrated in Fig. 1, a V-flame is stabilized by a 1.5-mm rod located 10 mm downstream of the burner surface and 2 mm to one side of the centerline. Both premixed ($\phi_1 = \phi_2$) and stratified ($\phi_1 < \phi_2$) flames have been studied.

Table 1 lists flame conditions for the cases investigated at Sandia. Stratification ratios (ϕ_2 / ϕ_1) range from 1.0 (uniformly premixed) to 3.0, with the overall equivalence ratio being 0.73 in all cases. Various levels of turbulence were achieved using two overall flow rates and two burner exit configurations (with and without a square grid at the burner surface). With the grid in place the measured profiles of mean velocity and turbulence intensity are reasonably uniform across the measurement region [12]. With the grid removed, the flow field is no longer uniform. However, turbulence intensities are higher, causing a higher degree of flame wrinkling and stronger flow-flame interaction, allowing for evaluation of the present diagnostics over a broader range of conditions.

2.2. Diagnostic system and data analysis

The facility for multiscalar measurements has been described previously [13-15]. It combines line imaging of spontaneous Raman scattering, Rayleigh scattering, and two-photon LIF of CO, in order to obtain single-shot profiles of temperature and the concentrations of major species (CO_2, O_2, CO, N_2, CH_4, H_2O, and H_2). The beams from four frequency-doubled Nd:YAG lasers were used for Raman and Rayleigh line imaging, yielding a total energy of 1.8 J/pulse in the probe volume. Optical delay lines were used to temporally stretch each pulse to avoid optical breakdown at the focus, which had a diameter of ~0.22 mm ($1/e^2$). CO was excited at 230.1 nm (two photons), with the UV laser beam aligned on the same axis as the Nd:YAG laser beams.

A new optical collection system for line-imaged Raman, Rayleigh, and CO-LIF measurements was recently developed [16] and was applied here to turbulent flames for the first time. As illustrated in Fig. 2, CCD cameras for Raman, Rayleigh, and CO-LIF were combined into one unit. A pair of 150-mm diameter achromats (Linos Photonics, *f*/2 and *f*/4) imaged a

portion of the laser beam into this detection unit. The main internal components included two custom-built, motor-driven chopper wheels, six commercial camera lenses, a custom transmission grating (Kaiser Optical), and mirrors and filters to separate and isolate the light signals for Raman scattering (~550-700 nm), Rayleigh scattering (532 nm), and CO fluorescence (~480-488 nm).

The two chopper wheels were locked in frequency and phase to a master controller, which also generated timing signals for the lasers and cameras. The "slow" wheel (3000 rpm, 300 μs FWHM gate) was located at the focus of the collection lens. Relay lens pairs and beam splitters separated the wavelengths of interest and refocused the respective images onto the Rayleigh detector, the intensified CO-LIF detector, and the stationary slit of the "fast" wheel (21000 rpm, 3.9 μs FWHM gate) for the Raman detector. The CCD cameras were the same as used in the previous collection/detection setup, with the non-intensified, low-noise, cryogenically-cooled Raman detection array (Princeton Instruments VersArray 1300B with CryoTiger cooling unit) being most critical for the overall system.

The spacing of binned superpixels along the laser axis was 0.104 mm, 0.020 mm, and 0.101 mm, for the Raman, Rayleigh, and CO-LIF measurements, respectively. The optical resolution was determined primarily by the pair achromatic lenses at the front end of the collection system, and Zemax calculations of this lens system show essentially all rays falling within a radius of 0.075 mm after 2:1 magnification. Details of the optical design and performance are given in [16].

Planar imaging of OH fluorescence from two crossed laser sheets that intersect along the multiscalar measurement line was used to determine the 3D orientation of the flame [13,14]. In the present work, 10-element UV lenses (CERCO 45 mm f/1.8) were combined with intensified CCD cameras (Andor). The imaged region for each plane was 10 mm by 8 mm with each pixel

corresponding to 0.150 mm in the flame. The OH images were processed by subtracting an averaged background frame, applying an average sheet correction based on measurements in products 3 cm above a premixed CH_4/air flat flame at near adiabatic conditions, applying a 5x5 Gaussian filter to reduce noise, applying an edge detection algorithm, fitting polynomials through the edge pixels in each plane in the region near the intersecting line, calculating the tangent and normal vectors in each plane, and then calculating the 3D flame normal vector. In the present work we only present example image pairs. Future work will include analysis of statistics on flame orientation and curvature.

Calibrations for the line-imaged measurements were based on cold flows, heated flows, laminar jet diffusion flames, and flat CH_4/air flames of known composition. Table 2 lists uncertainties at representative conditions, based on the standard deviations (precision) and estimated accuracy of averaged measurements. Estimates of accuracy were based on uncertainties in calibration flow conditions and repeatability of measurement. All flows were measured using mass flow controllers that were calibrated (within 1% of reading) against laminar flow elements. There may be additional errors in the scalar measurements associated with the effects of spatial averaging across steep scalar gradients, and this issue is addressed in the next section.

3. Results and discussion

Representative results are presented below to illustrate the capabilities and limitations of these combined diagnostics as applied to premixed and stratified flames. Some discussion of physical processes is included. However, detailed analysis of the statistical properties of these flames is beyond the scope of the present paper and will only be outline in the context of future

work. One important observation is that the gradient in equivalence ratio can be significant within the scale of the thermal flame thickness. This result calls into question the common modeling assumption that stratified flames may be represented as an ensemble of premixed flames, and it highlights the importance of detailed scalar measurements in stratified flames.

3.1. Average profiles of ϕ and T

Profiles of mean and fluctuating temperature and equivalence ratio reveal the location and width of the flame brush and stratified mixing layer. Example Reynolds average profiles are shown in Fig. 3 for $z = 25$ mm downstream of the burner surface in flames fs1 and fs6, the premixed and most stratified cases in the series with square grid and lower flow rates (see Table 1). These profiles were obtained by translating the ~6-mm probe volume through each flame in overlapping 3-mm steps, with 500 shots acquired at each step. There are slight discontinuities at 3-mm intervals in the profiles, which result from differences in optical throughput and detection across the measurement region that are not corrected completely by the present scheme of calibrations and data processing. Improvements are possible using data processing methods that are under development (in collaboration with A. Dreizler, F. Fuest and D. Geyer, Technical University of Darmstadt). Note that Favre (density weighted) statistics may also be determined from these measurements.

Results from the premixed flame demonstrate that there is relatively little error in the measured equivalence ratio either within the flame, where the instantaneous temperature gradient exceeds 2000 K/mm, or in the post-flame gasses, where spatial resolution is not an issue but errors in species measurements translate to errors in equivalence ratio. The measured equivalence ratio in the products is too high by roughly 0.02, compared to the value of 0.73 in the reactants. Fluctuations in the measured equivalence ratio are below 2% in the fully burnt

portion of the profile and increase slightly within the flame brush to about 3%. These errors are relatively small compared to the fluctuation levels in the stratified flame.

In the stratified flame (fs6, Fig. 3b) the center of the flame brush has nearly reached the midpoint in the scalar mixing layer at this downstream location of z = 25 mm. The midpoint in the mixing layer is where $\bar{\phi}$ = 0.73 (solid line in Fig. 3b), and the center of the flame brush is taken as the maximum in T'. A few things are apparent from these profiles. First, the stratified flame has progressed further outward than the premixed flame at this downstream location. While stratification may have important effects on the local turbulent burning rate, it is also true that flame fs6 burns through mixtures with higher laminar flame speeds for most of the distance up to the measurement location. Second, the center of mixing layer is displaced from the centerline of the burner, and it is not symmetric, as in the corresponding nonreacting flow (not shown). Both effects result from volume expansion through the flame, which causes an outward deflection of the mean flow and a stretching of the $\bar{\phi}$ profile on the burnt side of the flame. Third, the peak in ϕ' occurs toward the unburnt side of the mixing layer near x = -5 mm, where the maximum gradient in $\bar{\phi}$ occurs.

3.2. Resolution of premixed flame structure

A central issue for any measurement of premixed or stratified flames is whether the diagnostic technique has sufficient spatial resolution to accurately probe the structure of thin flames. This issue is first addressed by comparing measured and calculated profiles temperature and its gradient in a low-stretch premixed flame. For this purpose, a single realization from the premixed flame with lowest turbulence levels (fs1) was selected, based on the crossed OH PLIF images. The selected realization has low curvature in both planes and a calculated 3D flame

normal within 9 degrees of the multiscalar measurement line, corresponding to a cosine error of 1% in the gradient along the measured projection. The measured instantaneous profiles of temperature and its gradient (by central differencing) are plotted in Fig. 4 along with calculated profiles for unstrained flames at equivalence ratios of 0.73 and 0.75, giving an indication of the sensitivity of the gradient to uncertainty in the equivalence ratio. Calculations were performed using Chemkin 3 with the GRI 3.0 mechanism. Agreement is quite good between the measured profiles and the calculation at $\phi = 0.73$, with the maximum in the measured gradient being attenuated only slightly by central differencing at the experimental resolution.

The capability of the present system to measure species profiles within thin reaction zones is demonstrated in Fig. 5, where scatter plots of species mole fractions and the measured equivalence ratio are plotted vs. temperature for a set of 500 laser shots at a downstream distance of 25 mm in the premixed flame fsh1 (square grid, higher flow rates). The solid line in each frame shows the result of an unstrained calculation at $\phi = 0.73$. Plotting results in this way emphasizes the internal structure of the flame. In general, measurements follow the laminar calculation. Results for CO are particularly encouraging, given the importance of CO as a regulated pollutant. However, there are some areas of disagreement. Measurements of ϕ are again too high by about 0.02 (3%) in the burnt products. The measured H_2 levels are clearly higher on average than in the laminar calculation, and this difference is consistent across all measurements in the turbulent premixed flames studied here. Uncertainty, in the H_2 calibrations is estimated to be roughly 10% or less for temperatures up to 800 K and near 2000 K, which cannot explain the difference observed in Fig. 5. Levels of flame luminosity and fluorescence interference are very low in these experiments and do not contribute to the observed high H_2 results. (Note to reviewers: Effects of flame stretch have not yet been considered. Comparisons

with strained flame calculations are planned, so additional information on this issue will be available before publication.)

3.3. Stratified flame structure

Scatter plots of measured scalars in the stratified flames give a very different visual impression than those from the premixed flame. In Fig. 6, results from three different positions of the probe are displayed for a total of 1500 laser shots (roughly 87000 individual point measurements). Six curves corresponding to unstrained laminar flame calculations at equivalence ratios of $\phi = 0.6, 0.7, ..., 1.1$ are also plotted. It is obvious that this stratified flame exhibits a broad range of conditions within the reaction zones. The full range of equivalence ratios, $0.37 < \phi < 1.10$, is represented in samples near 300 K, and it is apparent from the results for CH_4 and ϕ that the preheat zone can reach all the way to mixtures at $\phi = 0.37$, even though this is below the flammability limit. Furthermore, the lower bounds on the scatter data for CH_4 and ϕ suggest that there can be significant changes in ϕ within the preheat zone of these stratified flames because CH_4 is consumed at conditions above or near the calculated curve for $\phi = 0.6$. There are also interesting trends at higher temperatures and higher equivalence ratios. The mole fractions of CO and H_2 increase sharply at the highest temperatures. These "tails" in the scatter plots correspond to measurements in the fuel-rich combustion products (up to $\phi = 1.10$) that are adjacent to the flame brush.

The presence of significant gradients in ϕ within the instantaneous structure of these turbulent stratified flames is confirmed by single-shot realizations. Examples of single-shot profiles of ϕ, X_{CO}, and T are plotted in Fig. 7 along with the corresponding crossed OH PLIF images. The first example (labeled #99) shows a flame near the center of the probe volume that

is burning from rich to lean. The gradient in ϕ through which the flame is propagating is roughly 0.25/mm, and higher gradients are not uncommon. Marzouk et al. [17] performed calculations of unsteady laminar flames propagating through gradients in equivalence ratio and observed that such flames can have a substantially different response from uniformly premixed flames. They reported that flames burning through a negative gradient in ϕ burn faster and propagate into leaner mixtures than corresponding flames in uniform mixtures, due to a back-supported structure that increases temperature and radical concentrations in the reaction zone. The local mixture gradient can be negative, near zero, or positive in a turbulent stratified flame.

The second example (Fig. 7, #526) shows that the turbulent flow has folded a very lean finger of reactants into the flame brush, while the instantaneous flame front has propagated though a region at higher equivalence ratio. The flame speed at the edge of the lean pocket (toward the right side of the line graph) is expected to be very low compared to that of the flame near x = -7 mm, where ϕ is about 0.95. This potential for strong interaction of the mixing field with the dynamics of the local flame propagation is a central aspect of stratified flames that is not currently addressed by models.

3.3. Future work

Results presented above have demonstrated the capabilities of this combined diagnostic system for measuring the scalar structure of turbulent stratified flames. Of particular importance is the ability to measure the temperature and equivalence ratio within the flame. This will allow calculation of the local progress variable, $c = (T - T_u)/(T_{b,\phi} - T_u)$, where T_u is the unburnt temperature and $T_{b,\phi}$ is the adiabatic equilibrium temperature for the locally measured value of ϕ. Future work will involve analysis of various joint and conditional statistics of the measured

quantities, so that differences between stratified flames and uniformly premixed flames may be better understood. We will also investigate methods and limitations of determining flame-normal gradients in the progress variable from the present data. This could lead to information on instantaneous and conditional mean scalar dissipation in turbulent stratified flames, which is important for models.

4 Conclusions

The combination of line-imaged Raman/Rayleigh/CO-LIF and crossed planar OH LIF imaging was applied to turbulent stratified CH_4/air flames stabilized above a slot burner. A new detection system for the line-imaged measurements allowed measurements of major species, temperature, and equivalence ratio with a data spacing of 0.104 mm. Results for temperature, temperature gradient, and major species mole fractions in a low-stretch turbulent flame were in good agreement with an unstrained laminar calculation. Fluctuations in the measured equivalence ratio were below 2% in the premixed flame products and increase slightly within the turbulent flame brush to about 3%, giving assurance that instantaneous profiles of equivalence ratio in the stratified flames were measured with useful accuracy. Scatter plots of measured scalars in the turbulent stratified flames revealed a wide range of conditions. The scatter data for CH_4 mole fraction and equivalence ratio vs. temperature suggested that significant gradients in equivalence ratio can occur within the thermal thickness of turbulent stratified flames. The presence of such gradients was confirmed in single-shot profiles. This result calls into question the common modeling assumption that turbulent stratified flames may be represented as an ensemble of premixed flames at different equivalence ratios, and further work is needed to

determine the quantitative significance of this new insight on the scalar structure of stratified flames.

Acknowledgments

Sandia contributions to this research were supported by the Division of Chemical Sciences, Geosciences and Biosciences, Office of Basic Energy Sciences, US Department of Energy. Sandia National Laboratories is a multiprogram laboratory operated by Sandia Corporation, a Lockheed Martin Company, for the United States Department of Energy under contract DE-AC04-94-AL85000. PAF was supported by the Brazilian Council for Scientific and Technological Development (CNPq) and Rolls-Royce. SH acknowledges additional support from the Wolfson Merit Award from the Royal Society. A visit by RSB to the University of Cambridge was supported by a Distinguished Visiting Fellowship grant from the Royal Academy of Engineering. Contributions by R. Harmon in support of these experiments are gratefully acknowledged.

References

[1] H.C. Mongia, AIAA Paper (1998) 98–3982.

[2] F. Q. Zhao, M. C. Lai and D. Harrington, Prog. Energy Combust. Sci. 25 (1999) 437–562.

[3] W. Meier, P. Weigand, X.R. Duan, R. Giezendanner-Thoben, Combust. Flame 150 (2007) 2–26.

[4] A.X. Sengissen, J.F. Van Kampenb, R.A. Huls b, G.G.M. Stoffels, J.B.W. Kok, T.J. Poinsot, Combust. Flame 150 (2007) 40–53.

[5] C. Duwig, C. Fureby, Combust. Flame 151 (2007) 85–103.

[6] Z. Tan, R.D. Rietz, SAE Paper 2004-01-0102 (2004).

[7] D.C. Haworth, R.J. Blint, B. Cuenot, T.J. Poinsot, Combust. Flame 121 (2000) 395–417.

[8] C. Jiménez, B. Cuenot, T. Poinsot, D. Haworth, Combust. Flame 128 (2002) 1–21.

[9] S. Shiga, S. Ozone, H.T.C. Machacon, T.Karasawa, H. Nakamura, T. Ueda, N. Jingu, Z. Huang, M. Tsue, M. Kono, Combust. Flame 129 (2002) 1–10.

[10] B. Renou, E. Samson, A. Boukhalfa, Combust. Sci. and Tech. 176 (2004) 1867–1890.

[11] N.Pasquier, B. Lecordier, M. Trinité, A. Cessou, Proc. Combust. Inst. 31 (2007) 1567–1574.

[12] P. Anselmo-Filho, R.S. Cant, S. Hochgreb, R.S. Barlow, Proc. Combust. Inst. 32 (submitted).

[13] A.N. Karpetis, T.B. Settersten, R.W. Schefer, R.S. Barlow, Optics Letters 29, (2004) 355–357.

[14] A.N. Karpetis, R.S. Barlow, Proc. Combust. Inst. 30 (2005) 665–672.

[15] G.H. Wang, A.N. Karpetis, R.S. Barlow, Combust. Flame 148 (2007) 62–75.

[16] G.H. Wang, U.D. Lee, D. Sunnarborg, C.R. Carlen, R.S. Barlow, "A rotating shutter based line Raman/Rayleigh/LIF Imaging System for Scalar Gradient Measurements in Turbulent Reacting Flows," paper in preparation.

[17] Y.M. Marzouk, A.F. Ghoniem, H.N. Najm, Proc. Comb. Inst. 28 (2000) 1859–1866.

Table 1

Flame designations and flow rates at 1 atm, 294 K

Flame[a]	ϕ_1	ϕ_2	ϕ_2/ϕ_1	CH_4 flow 1 (l/min)	CH_4 flow 2 (l/min)	air flows[b] (l/min)
fs1, fn1	0.73	0.73	1.00	6.58	6.58	85.0
fs4, fn4	0.51	0.95	1.86	4.61	8.55	85.0
fs6, fn6	0.37	1.10	3.00	3.29	9.87	85.0
fsh1, fnh1	0.73	0.73	1.00	8.82	8.82	116
fsh4, fnh4	0.51	0.95	1.86	6.18	11.5	116
fsh6, fnh6	0.37	1.10	3.00	4.41	13.2	116

[a] s – square grid, n – no grid, h – higher flow rates

[b] Air flows given for pairs of slots, including the coflow air slots

Table 2

Representative uncertainties in scalar measurements at flame conditions

Scalar	Precision, σ	Accuracy	Premixed flame
T	0.75%	2%	$\phi = 0.97$, $T = 2185$
N_2	0.7%	2%	"
CO_2	3.2%	4%	"
H_2O	2.4%	3%	"
ϕ	2.2%	5%	"
CO	4.5%	10%	$\phi = 1.28$, $T = 2045$
H_2	7.5%	10%	"

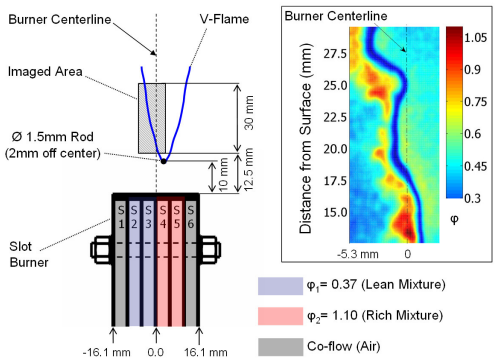

Fig. 1. Diagram of the stratified slot burner showing a rod-stabilized V-flame with one side intersecting the turbulent mixing layer between reactant streams of methane and air having two different equivalence ratios, ϕ_1 and ϕ_2. The inset shows simultaneous planar images of OH fluorescence from combustion products in the interior of the V-flame and acetone fluorescence in the cold reactant streams [12]. There dark blue gap between the acetone (left) and OH (right) sides of the combined image, which corresponds to intermediate temperatures within the reaction zone. The color scale corresponds to the equivalence ratio in the room-temperature reactants.

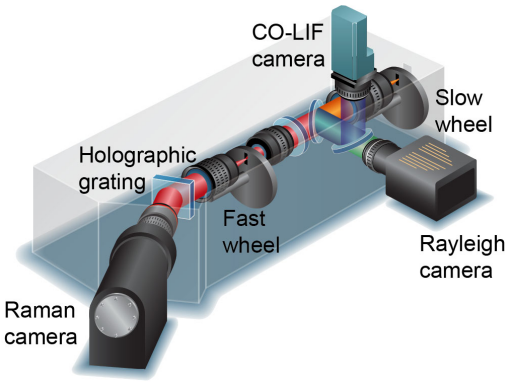

Fig. 2. Illustration of the main optical components of the light collection and detection system for combined Raman/Rayleigh/CO-LIF line-imaging.

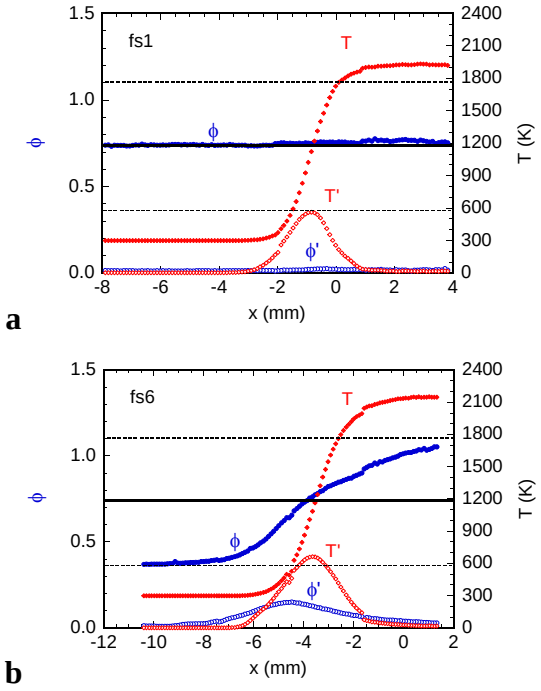

Fig. 3. Reynolds average profiles of mean and fluctuating equivalence ratio and temperature in flames fs1 (a) and fs6 (b) using the square grid and the lower flow rates. Profiles are from z = 25 mm downstream of the grid. The solid horizontal line is at $\phi = 0.73$, and the dashed lines are at $\phi = 0.37$ and 1.1, the boundary conditions of the stratified mixing layer in flame fs6. The x-axis origin corresponds to the center of the burner.

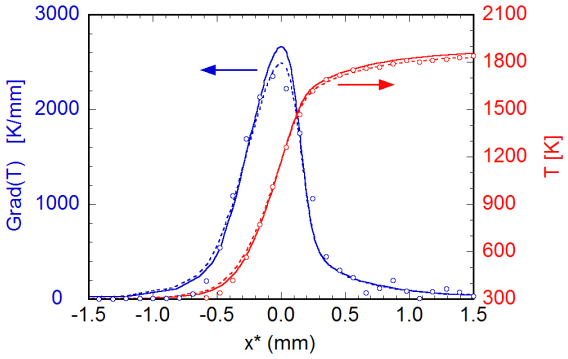

Fig. 4. Measured single-shot profiles of temperature and its gradient (symbols) compared with unstrained flame calculations at $\phi = 0.73$ (dashed lines) and $\phi = 0.75$ (solid lines). The coordinate x* is the distance from the location of the maximum temperature gradient.

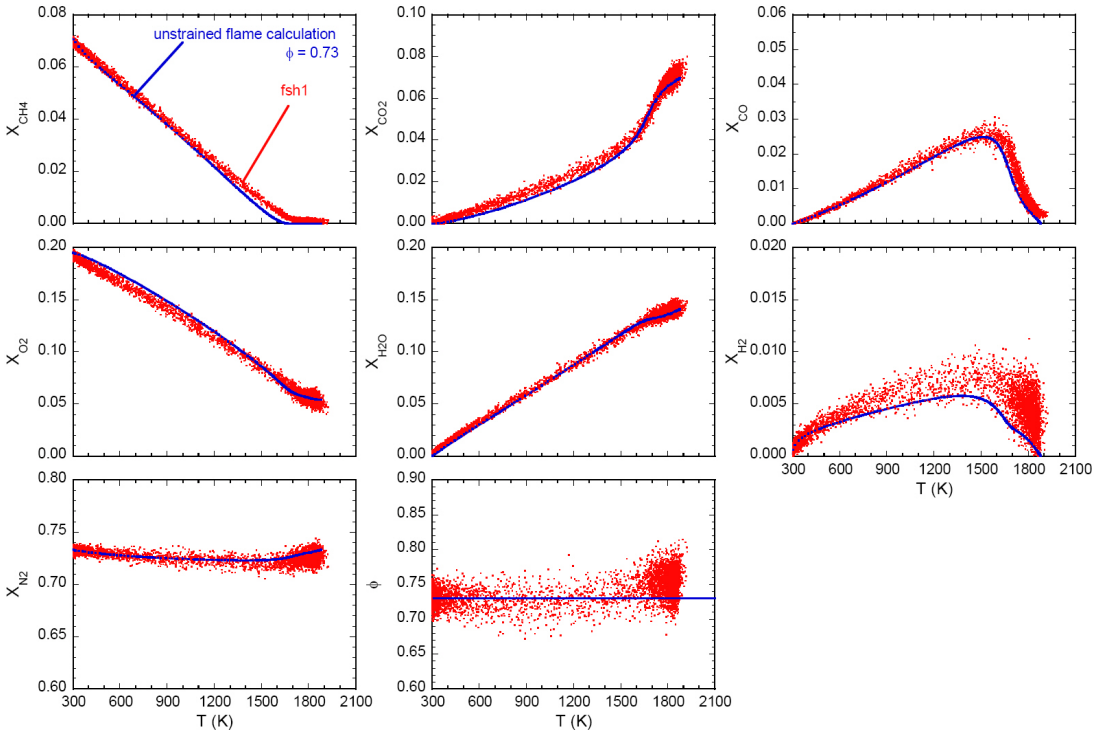

Fig. 5 Scatter data for mole fractions and equivalence ratio in flame fsh1 with the probe centered at z = 25 mm, x = -1.0 mm. Lines represent an unstrained flame calculation with ϕ = 0.73.

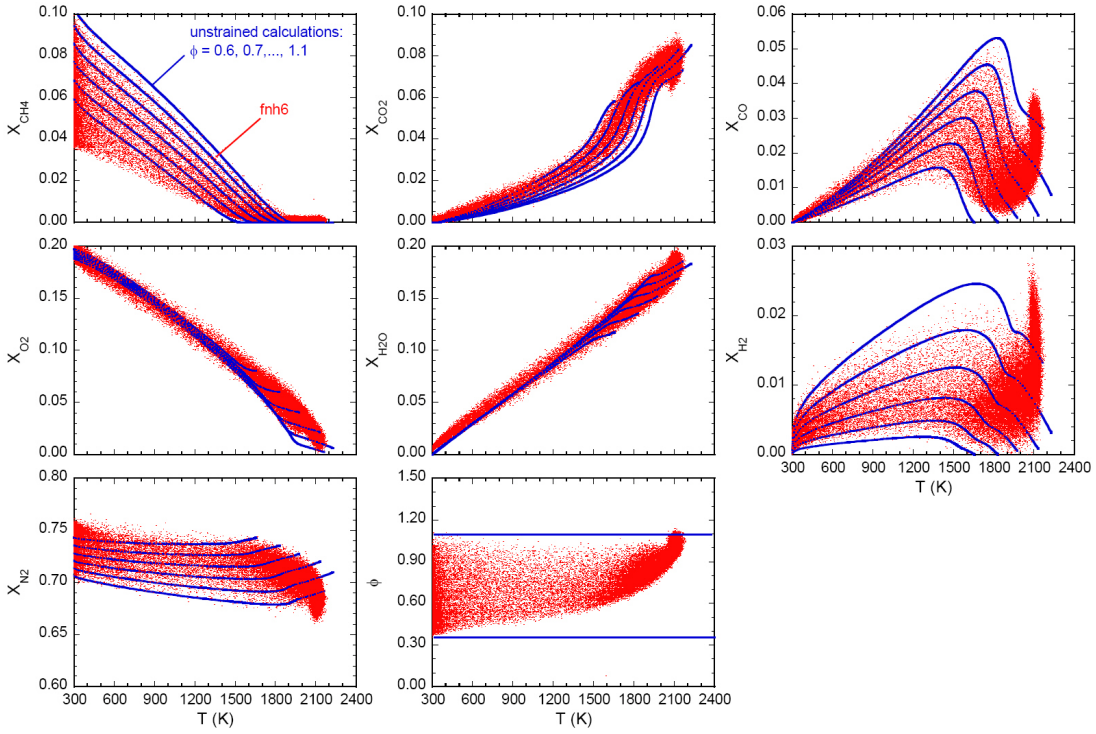

Fig. 6 Scatter data for mole fractions and equivalence ratio at z = 25 mm in flame fnh6. Lines represent unstrained flame calculations with ϕ = 0.6, 0.7,…, 1.1. Lines in the graph of ϕ mark values on the two sides of the stratification layer, ϕ_1 = 0.37 and ϕ_2 = 1.10.

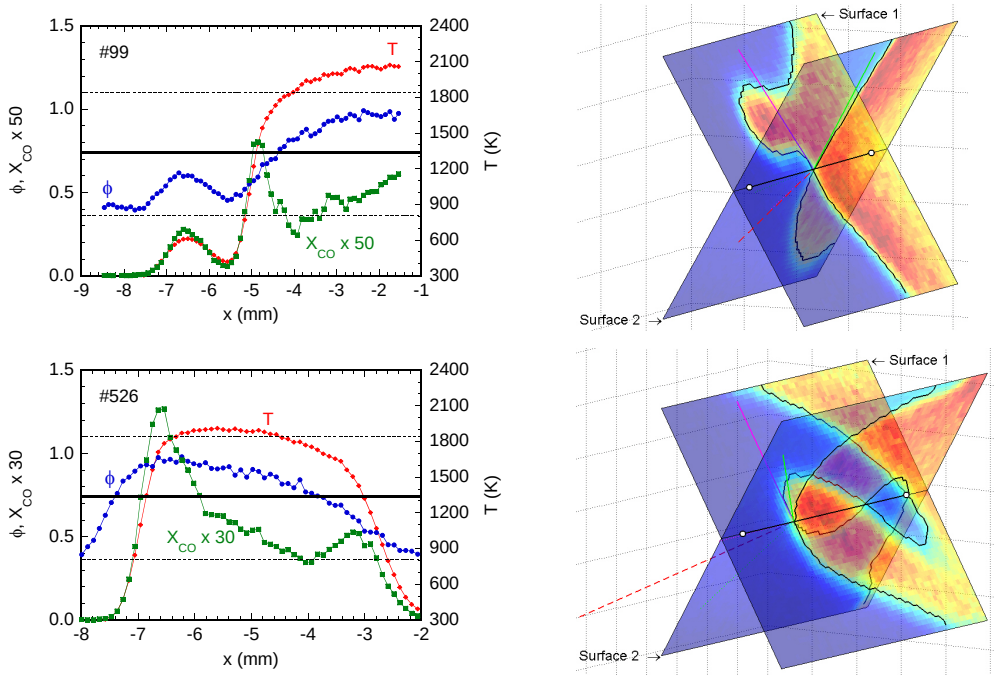

Fig. 7. Numbered single-shot examples of line measurements from flame fnh6 with the center of the measurement at $z = 25$ mm downstream and $x = 5$ mm from the burner centerline. Corresponding crossed OH PLIF images are shown as 3D projections. The black curves mark the detected edges from which flame curvature in each plane and the 3D flame normal vector may be determined. The bold line along the intersection marks the 7-mm extent of the multiscalar line images; results from the center 6 mm are plotted.

Figure Captions:

Fig. 1. Diagram of the stratified slot burner showing a rod-stabilized V-flame with one side intersecting the turbulent mixing layer between reactant streams of methane and air having two different equivalence ratios, ϕ_1 and ϕ_2. The inset shows simultaneous planar images of OH fluorescence from combustion products in the interior of the V-flame and acetone fluorescence in the cold reactant streams [12]. There dark blue gap between the acetone (left) and OH (right) sides of the combined image, which corresponds to intermediate temperatures within the reaction zone. The color scale corresponds to the equivalence ratio in the room-temperature reactants.

Fig. 2. Illustration of the main optical components of the light collection and detection system for combined Raman/Rayleigh/CO-LIF line-imaging.

Fig. 3. Reynolds average profiles of mean and fluctuating equivalence ratio and temperature in flames fs1 (a) and fs6 (b) using the square grid and the lower flow rates. Profiles are from z = 25 mm downstream of the grid. The solid horizontal line is at $\phi = 0.73$, and the dashed lines are at $\phi = 0.37$ and 1.1, the boundary conditions of the stratified mixing layer in flame fs6. The x-axis origin corresponds to the center of the burner.

Fig. 4. Measured single-shot profiles of temperature and its gradient (symbols) compared with unstrained flame calculations at $\phi = 0.73$ (dashed lines) and $\phi = 0.75$ (solid lines). The coordinate x* is the distance from the location of the maximum temperature gradient.

Fig. 5 Scatter data for mole fractions and equivalence ratio in flame fsh1 with the probe centered at z = 25 mm, x = -1.0 mm. Lines represent an unstrained flame calculation with ϕ = 0.73.

Fig. 6 Scatter data for mole fractions and equivalence ratio at z = 25 mm in flame fnh6. Lines represent unstrained flame calculations with ϕ = 0.6, 0.7,…, 1.1. Lines in the graph of ϕ mark values on the two sides of the stratification layer, ϕ_1 = 0.37 and ϕ_2 = 1.10.

Fig. 7. Numbered single-shot examples of line measurements from flame fnh6 with the center of the measurement at z = 25 mm downstream and x = 5 mm from the burner centerline. Corresponding crossed OH PLIF images are shown as 3D projections. The black curves mark the detected edges from which flame curvature in each plane and the 3D flame normal vector may be determined. The bold line along the intersection marks the 7-mm extent of the multiscalar line images; results from the center 6 mm are plotted.